IEEE Access
Multidisciplinary | Rapid Review | Open Access Journal

Received March 14, 2019, accepted March 29, 2019, date of publication April 4, 2019, date of current version April 16, 2019.

Digital Object Identifier 10.1109/ACCESS.2019.2909308

Sensorless Vector Control of Permanent Magnet Synchronous Linear Motor Based on Self-Adaptive Super-Twisting Sliding Mode Controller

ZHENG LI, (Member, IEEE), SHUO ZHOU, YU XIAO, AND LEIYONG WANG
School of Electrical Engineering, Hebei University of Science and Technology, Shijiazhuang 050018, China

Corresponding author: Zheng Li (lzhfgd@163.com)

This work was supported in part by the National Natural Science Foundation of China under Grant 51577048, Grant 51877070, and Grant 51637001, in part by the Hebei Provincial Natural Science Foundation Project under Grant E2018208155, in part by the Hebei Province Overseas Students Science and Technology Activity Project Selected Project under Grant C2015003044, in part by the Hebei Province Higher Education Science and Technology Research Key Project under Grant ZD2018228, in part by the High-Energy-Saving Motor and Control Technology National and Local Joint Engineering Laboratory Open Project Funded Project under Grant KFKT201804, and in part by the Hebei Province Graduate Innovation Funding Project under Grant CXZZSS2018085.

ABSTRACT Due to its own structural characteristics, permanent magnet synchronous linear motors (PMSLMs) have unstable motor parameters during operation due to the end effect and the inherent magnetic circuit instability. At the same time, linear motors have the characteristics of reciprocating switching motion and high-speed positioning motion in industrial applications, thus placing high demands on the controller. In order to improve the performance of the PMSLM, this paper firstly studies the linear motor structure, the distribution characteristics of its air gap magnetic field are obtained, and the simulation analysis for the back electromotive force (EMF) of PMSLM of its running process is carried out. Then, a state observer based on the sliding mode state observer (SMO) is built to replace the traditional speed sensor and a super-twisting sliding mode controller is designed. The double-closed loop control of the speed and the use of high-order sliding mode control features effectively reduce the chattering of the system and reduce the impact of the observation error brought by the observer on the system. The adaptive sliding mode control strategy is used to effectively suppress the influence of the boundaryless uncertainty interference on the system and reduce the influence of the observation error brought by the observer on the system. This paper also combines the linear motor experimental platform to further verify the control scheme based on the super-twisting sliding mode non-sensing linear motor. The simulation and experimental results show that SMO has accurate speed and position tracking performance, the system's chattering is significantly reduced, the control precision is excellent, and the introduction of adaptive sliding mode controller enhances the robustness of the system.

INDEX TERMS Self-adaptive super-twisting sliding mode controller (self-adaptive ST-SMC), sliding mode state observer (SMO), linear motor, magnetic field vector control, finite element analysis.

I. INTRODUCTION

As high speed, high precision technology, high performance industry rapidly developing, permanent magnet synchronous linear motors (PMSLM) for highly efficient, high precision, low power consumption, high thrust, rapid response, easy to control the significant advantages, broad prospects for development, in the nc machine tools, aerospace industry, industrial robots, and other areas of the electrical drive has huge development potential of the [1]–[4]. With the development of microcomputers, the emergence of high-performance DSP has promoted the application of the complex control algorithm in motor control. In the [5], a speed controller based on model predictive control is designed. The disturbance observer is used to estimate the system disturbance, and the torque current compensation amount is generated according

The associate editor coordinating the review of this manuscript and approving it for publication was Zheng Chen.

to the feedforward correction of the control amount, so as to achieve the disturbance suppression. Both are disturbance observer based compensation control methods, which consider model uncertainties, modeling errors and load torques as concentrated disturbances, and estimate and dynamically compensate them. At the same time, the sliding mode variable structure algorithm has been developed rapidly in recent years due to its simple structure and strong operability. In the [6], the author designed an adaptive sliding mode algorithm, combined with the sliding mode algorithm for finite time convergence and adaptive algorithm. Solving the advantages of the uncertainty boundary problem, good results have been achieved in the control application of brushed motors. In the [7], the application of high-order sliding mode in the field of permanent magnet synchronous motor control is discussed. The theoretical development of high-order sliding mode control in traditional sliding mode is to avoid jitter while maintaining the main advantages of SMC. This control technique extends the traditional sliding mode control idea by replacing the first derivative acting on it with the time derivative acting on the higher order sliding mode variable. The implementation of high-order SMC requires an effective sliding variable derivative. This scheme is highly robust, which makes it attractive for drive control research. The literature [8] mainly studies the second-order sliding mode theory and its application characteristics, and provides a proof method for proving the stability of the second-order sliding mode controller. The second-order sliding mode has been widely used for its outstanding control advantages. In [9], [10], using the state observer principle, a reduced-order state observer, a sliding mode observer, an extended Kalman observer and a full-dimensional state observer are designed to observe the rotor position of the motor. Among them, the sliding mode observer has the characteristics of fast convergence and good engineering realization compared with other observers. Other full-dimensional state observers such as the Kalman observer have the disadvantages of huge computational complexity and difficult engineering realization. In this paper, a sliding mode state observer (SMO) is designed. Based on the error between the given current and the observed current, a position-free sensing control strategy is constructed. Using the sliding mode state observer to observe the back EMF of PMSLM, not only the velocity and position of the mover can be obtained, but also the dynamic response is fast, easy to implement, and the robustness of the system is enhanced.

PMSLM is susceptible to edge effects and end effects caused by thrust fluctuations and uneven magnetic field distribution in the motor during operation. At the same time, because PMSLM directly drives the load, the change of the load during operation and the external disturbance received will directly affect the motor mover, thus greatly reducing the motion accuracy of the motor. In the sensorless control strategy, the observation error brought by the observer and the structural error caused by the overall control system are inevitable interference to the controller. This puts higher requirements on the control strategy of PMSLM. Sliding mode variable structure control is a simple structure with strong robustness to external disturbances, fast response, and discontinuity. In this paper, Super-twisting sliding mode control is introduced into the speed controller and current controller in vector control. Super-twising is a high-order sliding mode control method. On the basis of maintaining fast response and strong robustness of first-order sliding mode, it can not only further suppress thrust pulsation, but also effectively avoid or suppress "chattering" generated in the observer. The sliding mode control structure has good engineering achievability. It must have good anti-interference performance in the face of the change of electrical parameters and the harsh industrial environment during motor operation. In this paper, an adaptive sliding mode controller is introduced. In the face of undetermined boundary disturbance, the controller parameters can be adjusted in time, the disturbance effect is suppressed, and the system performance is improved. Finally, the control strategy and simulation results adopted are verified on the experimental platform of PMSLM. The results show that the sliding mode control strategy proposed in this paper can accurately track the switching motion of the linear motor system, and the dynamic response speed is fast and the control precision is excellent.

II. LINEAR MOTOR STRUCTURE ANALYSIS

The structure of the bilateral ironless permanent magnet synchronous linear motor is shown in Figure 1.

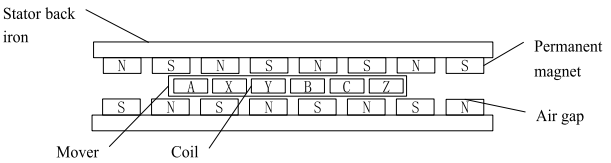

FIGURE 1. Structure of permanent magnet synchronous linear motor without core.

The iron-free permanent magnet synchronous linear motor is composed of a stator and a mover, and the stator part is composed of a permanent magnet and a back iron. The polarity distribution of the permanent magnet is as shown in Figure 1, because the upper and lower permanent magnets have opposite magnetic properties. The normal suction, so the permanent magnet needs to be fixed on the back iron by super glue, and in order to avoid deformation, the length of the stator should not be too long. There is no iron core in the three-phase windings in the mover, and it is packaged and fixed by epoxy resin. The alternating current generated by the sinusoidal law changes with time to generate a traveling wave magnetic field, which interacts with the static magnetic field generated by the permanent magnet to promote the movement of the mover. Since the mover has no iron core structure, there is no cogging force, and the end effect is much smaller, so that the linear motor does not have a positioning force, and the operation is more stable. The motor winding adopts

a 5-pole/3 coil structure, and the coils are closely arranged. It can effectively shorten the length of the mover and improve the efficiency of the mover.

A. AIR GAP MAGNETIC FIELD ANALYSIS

Accurate analysis of linear motors is best to establish a three-dimensional model of the motor, but the three-dimensional model is complex and the number of equations and the number of dimensions are large, which is not conducive to analytical calculation. In order to simplify the analysis process, the three-dimensional model is reasonable. Assuming that the calculation is simplified for a two-dimensional model, the following assumptions can be made [11]–[13]:

(1) Assume that the linear motor stator is infinitely long in the x-axis and z-axis directions;

(2) It is assumed that the magnetic permeability of the linear motor ferromagnetic material is infinite;

(3) Ignore the end effect caused by the magnetic field distortion at the end of the motor.

According to the above assumption, the complex linear motor three-dimensional magnetic field solving problem is simplified to the two-dimensional magnetic field solving problem. Since the air gap magnetic field in the permanent magnet synchronous linear motor is almost entirely provided by the permanent magnet, the air gap magnetic is solved by the analytical method. The permanent magnet needs to be equivalent. The principle of the equivalent magnetic potential method (EMPM) is to equivalent the permanent magnet into an infinitely thin coil, so that the magnetomotive force generated by the coil is equivalent to the magnetomotive force generated by the permanent magnet. The region composed of the permanent magnet and the air gap is equivalent to a passive field, and the magnetomotive force generated by the coil is used for calculation. The analytical model of the permanent magnet synchronous linear motor equivalent magnetic potential method is shown in Figure 2. , δ is the distance between the upper and lower stator back irons, that is, the air gap height [14]–[16].

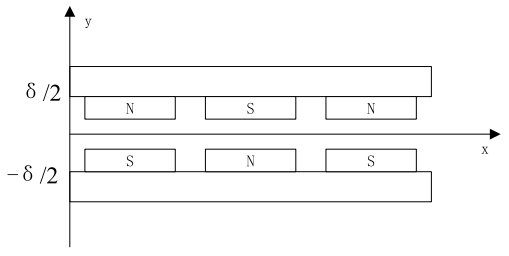

FIGURE 2. Linear motor analysis model.

Under the assumption that the magnetic field distribution of the permanent magnet is as shown in Figure 3, τ is the pole pitch of the linear motor, τ_{m} is the width of the permanent magnet, and the magnetic potential distribution function is as

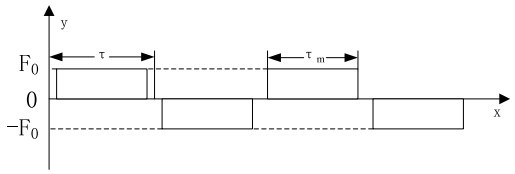

FIGURE 3. Equivalent magnetic potential distribution of permanent magnets.

shown in the formula (1).

$$F(x)=\begin{cases} F_0, & 2k\tau+\dfrac{t-t_m}{2}\le x\le(2k+1)-\dfrac{t-t_m}{2} \\ -F_0, & (2k+1)\tau+\dfrac{t-t_m}{2}<x<2(k+1)\tau-\dfrac{t-t_m}{2} \\ 0, & 2k\tau<x<2k\tau+\dfrac{t-t_m}{2}, \\ & (2k+1)\tau-\dfrac{t-t_m}{2}<x<(2k+1)\tau+\dfrac{t-t_m}{2}, \\ & 2(k+1)\tau-\dfrac{t-t_m}{2}<x<2(k+1)\tau \end{cases}$$

$$k=0,1,2,3\ldots \tag{1}$$

$$F_0=\frac{B_r}{\mu_0}h_m \tag{2}$$

where Br is the residual magnetic induction of the permanent magnet, μ_0 is the vacuum permeability, and h_m is the height of the permanent magnet. The magnetic potential distribution function can also be expressed as:

$$F(x)=\sum_{k=1}^{\infty}F_{mk}\sin\left(\frac{(2k-1)\pi}{\tau}x\right) \tag{3}$$

$$F_{mk}=\sum_{k=1}^{\infty}(-1)^{k+1}\frac{4}{(2k+1)\pi}F_0\sin\left(\frac{(2k+1)\pi\alpha_p}{2}\right) \tag{4}$$

$$\alpha_p=\frac{\tau_m}{\tau} \tag{5}$$

Since the area between the back irons is equivalent to a passive field, the scalar magnetic position there in satisfies the equation:

$$\nabla u(x,y)=\frac{\partial^2 u}{\partial x^2}+\frac{\partial^2 u}{\partial y^2}=0 \tag{6}$$

Using the variable separation method to solve the equation, the general solution of the equation is obtained:

$$u(x,y)=\sum_{k=1}^{\infty}(A_k\sin m_k x+B_k\cos m_k x)\,(C_k shm_k y+D_k chm_k y) \tag{7}$$

The scalar magnetic position is oddly symmetric about the x-axis, ie, the solution is taken into (7) to simplify the original equation as:

$$u(x,y)=\sum_{k=1}^{\infty}A_k\sin m_k x(C_k shm_k y+D_k chm_k y) \tag{8}$$

According to the hypothesis (2), the boundary conditions are:

$$u(x,y)\Big|_{y=\frac{\delta}{2}} = -u(x,y)\Big|_{y=-\frac{\delta}{2}} = -F(x) \tag{9}$$

Substituting equation (9) into equation (8) yields a system of equations:

$$\sum_{k=1}^{\infty} A_k \sin m_k x (C_k shm_k \frac{\delta}{2} + D_k chm_k \frac{\delta}{2}) = -\sum_{k=1}^{\infty} F_{mk} \sin\left(\frac{(2k-1)\pi}{\tau} x\right) \tag{10}$$

$$\sum_{k=1}^{\infty} A_k \sin m_k x \left(-C_k shm_k \frac{\delta}{2} + D_k chm_k \frac{\delta}{2}\right) = \sum_{k=1}^{\infty} F_{mk} \sin\left(\frac{(2k-1)\pi}{\tau} x\right) \tag{11}$$

$$m_k = \frac{(2k-1)\pi}{\tau} \tag{12}$$

The simultaneous equations (10), (11) are solved:

$$D_k = 0 \tag{13}$$

$$A_k \cdot Ck = -\frac{F_{mk}}{sh\left(m_k \frac{\delta}{2}\right)} \tag{14}$$

Substituting equations (13) and (14) into equation (8) yields:

$$u(x,y) = -\sum_{k=1}^{\infty} \frac{F_{mk}}{sh\left(m_k \frac{\delta}{2}\right)} \cdot shm_k y \cdot \sin m_k x \tag{15}$$

The general solution of the scalar magnetic position is obtained by partial derivation of x, y to obtain the component of the air gap magnetic density in the x, y direction:

$$B_x(x,y) = -\mu_0 \frac{\partial u(x,y)}{\partial x} = \sum_{k=1}^{\infty} \frac{\mu_0 m_k F_{mk}}{sh\left(m_k \frac{\delta}{2}\right)} \cdot shm_k y \cdot \cos m_k x \tag{16}$$

$$B_y(x,y) = -\mu 0 \frac{\partial u(x,y)}{\partial y} = \sum_{k=1}^{\infty} \frac{\mu_0 m_k F_{mk}}{sh\left(m_k \frac{\delta}{2}\right)} \cdot chm_k y \cdot \sin m_k x \tag{17}$$

B. FINITE ELEMENT METHOD VERIFICATION

In order to verify the accuracy of the air gap magnetic density expression obtained by the above analytical method, a two-dimensional finite element analysis(FEM) model of the permanent magnet synchronous linear motor is established, and the air gap magnetic density is solved and analyzed. The pole distance of the linear motor is $\tau = 16$mm. The permanent magnet has a high hm = 5mm, a permanent magnet width τ m = 13mm, an air gap height $\delta = 19.6$mm, and a winding height hc = 3.76mm. The obtained magnetic induction line distribution and air gap magnetic density distribution are shown in Figure 4.

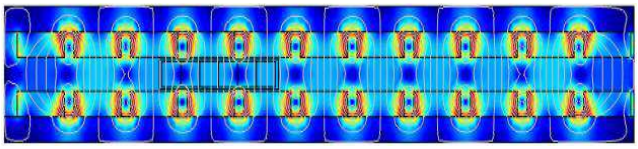

FIGURE 4. Distribution of magnetic line and magnetic flux density.

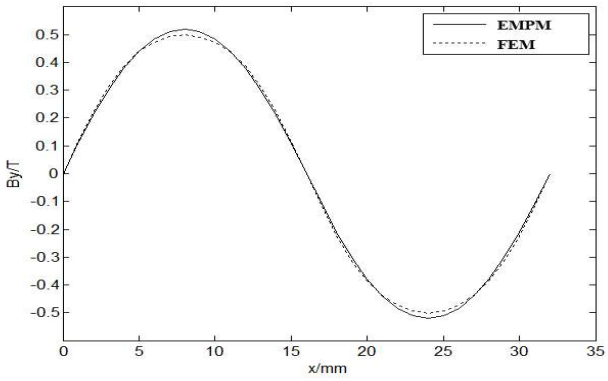

FIGURE 5. Air gap magnetic density distribution diagram at y = 0 mm stribution.

The air gap magnetic density obtained by the analytic method at y = 0 mm is compared with the air gap magnetic density obtained by the finite element method. The results are shown in Figure 5. It can be seen from the figure that the calculation result of the equivalent magnetic potential method only has a significant error in the peak and valley of the magnetic density curve. The calculated average error is 3.04%, and the accuracy meets the requirements.When modeling a linear motor, in order to facilitate the analysis and calculation, the appropriate assumption of the three-dimensional model is reduced to a two-dimensional model, so that the calculation result of the analytical method produces a certain error, but the error is small, which can be ignored.Therefore, it can be considered that the calculation accuracy of the analytical method satisfies the requirements.

III. MATHEMATICAL MODEL OF PMSLM BASED ON VECTOR CONTROL

The three-phase alternating current is passed into the stator winding of the PMSLM. At this time, the air-space traveling wave magnetic field generated in the stator winding interacts with the magnetic pole of the mover, and the generated electromagnetic thrust pushes the mover forward to move linearly. In the ideal state, the armature coils of the stator are evenly distributed, and the air gap magnetic field between the mover and the stator exhibits a sinusoidal distribution. At this time, the motor is always in a linear working state. During the control of the motor, magnetic saturation and external disturbance are ignored, and the back potential is assumed to be a sine wave. According to the magnetic field vector orientation control method of PMSLM, the coupling between speed and current is neglected. The mathematical model of linear motor mainly includes voltage balance equation, torque

equation and motion equation. After Clark transform and Park transform, the mathematical model in d-q coordinates is:

$$\begin{bmatrix} u_d \\ u_q \end{bmatrix} = R\begin{bmatrix} i_d \\ i_q \end{bmatrix} + \begin{bmatrix} L_d \\ L_q \end{bmatrix}\begin{bmatrix} \dot{i}_d \\ \dot{i}_q \end{bmatrix} - \begin{bmatrix} vL_q\frac{\pi}{\tau} \\ vL_d\frac{\pi}{\tau} \end{bmatrix}\begin{bmatrix} i_q \\ i_d \end{bmatrix} + \begin{bmatrix} 0 \\ v\psi_f\frac{\pi}{\tau} \end{bmatrix} \quad (18)$$

In the above formula, u_d and u_q represent the d and q axis voltages in the rotating coordinate system, R is the stator winding, i_d and i_q are the d and q axis currents in the rotating coordinate system, and L_d and L_q respectively correspond to the d and q axis inductances on the stator, τ is expressed as the pole distance, ψ_f is expressed as the magnetic pole flux of the mover, v is the linear velocity of the mover, and $v = \frac{\tau}{\pi}\omega$.

The current balance equation of PMSLM can be obtained by equation (1):

$$\begin{bmatrix} \frac{di_d}{dt} \\ \frac{di_q}{dt} \end{bmatrix} = -\begin{bmatrix} \frac{R_s}{L_d} \\ \frac{R_s}{L_q} \end{bmatrix}\begin{bmatrix} i_d \\ i_q \end{bmatrix} + \begin{bmatrix} \frac{L_q}{L_d}\frac{v\pi}{\tau} \\ \frac{L_d}{L_q}\frac{v\pi}{\tau} \end{bmatrix}\begin{bmatrix} i_q \\ i_d \end{bmatrix} + \begin{bmatrix} \frac{1}{L_d} \\ \frac{1}{L_q} \end{bmatrix}\begin{bmatrix} u_d \\ u_q \end{bmatrix} - \begin{bmatrix} 0 \\ \frac{\psi_f}{L_q}\frac{v\pi}{\tau} \end{bmatrix} \quad (19)$$

According to the law of conservation of energy, the electromagnetic power of the motor can be obtained as follows:

$$p_e = F_e v = \frac{3}{2}p\omega(\psi_d i_q - \psi_q i_d) \quad (20)$$

wherein F_e represents the electromagnetic thrust, ψ_d, ψ_q are the d-axis and q-axis flux linkages, and P is the pole logarithm.

Because $\psi_d = L_d i_d + \psi_f$, $\psi_q = L_q i_q$, the electromagnetic thrust equation can be obtained as follows:

$$F_e = p\frac{3\pi}{2\tau}[\psi_f i_q + (L_d - L_q) i_d i_q] \quad (21)$$

For hidden pole linear motors, there will often be $L_d = L_q$, so the electromagnetic thrust can be written as:

$$F_e = p\frac{3\pi}{2\tau}\psi_f i_q \quad (22)$$

In addition, the motor's motion balance equation is:

$$M\dot{v} = F_e - Bv - F_l \quad (23)$$

M is the mass of the mover and its applied load.

IV. SMO SLIDING MODE OBSERVER DESIGN

PMSLM uses the sliding mode observer to estimate the position and velocity of the mover based on the α-β two-phase stationary coordinate system in vector control. According to equation (2), the current balance equation under the SMO algorithm can be obtained as [17]–[19]:

$$\begin{bmatrix} \frac{di_\alpha}{dt} \\ \frac{di_\beta}{dt} \end{bmatrix} = \frac{1}{L_s}\begin{bmatrix} u_\alpha \\ u_\beta \end{bmatrix} - \frac{1}{L_s}\begin{bmatrix} e_\alpha \\ e_\beta \end{bmatrix} - \frac{R_s}{L_s}\begin{bmatrix} 1 \\ 1 \end{bmatrix} \quad (24)$$

In the above formula, i_α and i_β are the currents under the α and β axes, u_α and u_β are the voltage components under the α and β axes, Rs is the stator winding, Ls is the inductance in the stator, e_α and e_β are the back electromotive force components under the α and β axes, which can be expressed as:

$$\begin{bmatrix} e_\alpha \\ e_\beta \end{bmatrix} = \omega_r\psi_f\begin{bmatrix} -\sin\theta \\ \cos\theta \end{bmatrix} \quad (25)$$

It can be seen from the above equation that, in the case of assuming $L_d = L_q$, the back EMF is proportional to the equivalent rotational speed and position angle of the mover. After calculating the back EMF, the position angle and equivalent speed of the mover during motor motion can be obtained. Therefore, the value of the back EMF obtained by the observer is crucial. The position angle and equivalent speed of the mover can be expressed as:

$$\begin{cases} \theta = \arctan(-e_\alpha/e_\beta) \\ \omega = \sqrt{e_\alpha^2 + e_\beta^2}/\psi_f \end{cases} \quad (26)$$

When acquiring the back EMF, it is usually to reconstruct a system that is exactly the same as the original system. By observing the newly constructed system to obtain the required parameters, based on the original system, the state equation of the observer can be designed as:

$$\begin{bmatrix} \frac{d\hat{i}_\alpha}{dt} \\ \frac{d\hat{i}_\beta}{dt} \end{bmatrix} = -\frac{R_s}{L_s}\begin{bmatrix} \hat{i}_\alpha \\ \hat{i}_\beta \end{bmatrix} + \frac{1}{L_s}\begin{bmatrix} u_\alpha \\ u_\beta \end{bmatrix} - \begin{bmatrix} v_\alpha \\ v_\beta \end{bmatrix} \quad (27)$$

Among them, $\dot{\hat{i}}_\alpha$ and $\dot{\hat{i}}_\beta$ are the currents of α and β axes observed under the new system, and v_α and v_β are the sliding mode control laws adopted:

$$\begin{bmatrix} v_\alpha \\ v_\beta \end{bmatrix} = \frac{K}{L_s}\begin{bmatrix} \tanh(\hat{i}_\alpha - i_\alpha) \\ \tanh(\hat{i}_\beta - i_\beta) \end{bmatrix} \quad (28)$$

$$\tanh(ax) = \frac{e^{ax} - e^{-ax}}{e^{ax} + e^{-ax}} \quad (29)$$

In the control law designed by the above formula, the symbol function sgn(x) is replaced by the hyperbolic tangent function tanh(x). Since the hyperbolic tangent function is continuous smooth, using it as a switching function can effectively reduce chattering in sliding mode control. Control gain $K > \max\{\text{-R}|\hat{i}_\alpha - i_\alpha| + e_\alpha \tanh(\hat{i}_\alpha - i_\alpha), \text{-R}|\hat{i}_\beta - i_\beta| + e_\beta \tanh(\hat{i}_\beta - i_\beta)\}$.

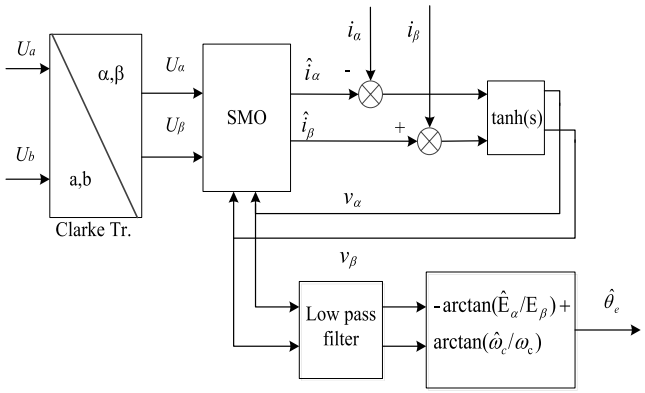

FIGURE 6. Schematic diagram of the sliding mode observer.

SMO is designed based on the error between the observed current and the original system current. Therefore, let equation (6) and equation (9) be poor, and the stator current error equation can be obtained:

$$\begin{bmatrix} \frac{d(\hat{i}_\alpha - i_\alpha)}{dt} \\ \frac{d(\hat{i}_\beta - i_\beta)}{dt} \end{bmatrix} = -\frac{R_s}{L_s}\begin{bmatrix} (\hat{i}_\alpha - i_\alpha) \\ (\hat{i}_\beta - i_\beta) \end{bmatrix} + \frac{1}{L_s}\begin{bmatrix} e_\alpha - v_\alpha \\ e_\beta - v_\alpha \end{bmatrix} \tag{30}$$

According to the above formula, the sliding surface can be directly set to: $s(x) = \hat{i} - i$, When the state variable reaches the sliding surface, $s(x) = \hat{i} - i = 0$, After that, the state variables $(\hat{i}_\alpha - i_\alpha)$ and $(\hat{i}_\beta - i_\beta)$ will remain on the sliding surface. The method of combining the equivalent control and the switching control in the sliding mode control, the control amount at this time can be equivalent to:

$$\begin{bmatrix} e_\alpha \\ e_\beta \end{bmatrix} = \begin{bmatrix} v_\alpha \\ v_\beta \end{bmatrix} = K\begin{bmatrix} \tanh(s(x)_\alpha) \\ \tanh(s(x)_\beta) \end{bmatrix} \tag{31}$$

Since the control amount at this time is a switching function with gain, in order to further reduce the chattering, a low-pass filter is added to the switching function in the equivalent process so that a continuous back EMF can be obtained, and:

$$\begin{bmatrix} \hat{e}_\alpha \\ \hat{e}_\beta \end{bmatrix} = \frac{\omega_c}{s + \omega_c} K\begin{bmatrix} \tanh(s(x)_\alpha) \\ \tanh(s(x)_\beta) \end{bmatrix} \tag{32}$$

where ω_c is the cutoff frequency of the low-pass filter.

When filtering the high-frequency switching signal, the result often results in phase and amplitude lag. This lag condition will directly affect the position angle of the acquired mover. At this time, it is necessary to add a certain angle compensation based on the obtained position angle to compensate for the phase angle delay caused by the low-pass filter, and the position angle of the phase-compensated mover is:

$$\begin{cases} \hat{\theta} = -\arctan(\frac{e_\alpha}{e_\beta}) + \arctan(\frac{\omega_r}{\omega_c}) \\ \omega_r = \dfrac{\sqrt{\hat{e}_\alpha + \hat{e}_\beta}}{\psi_f} \end{cases} \tag{33}$$

Based on the above formula, the block diagram of SMO implementation is shown in Figure 6. It mainly includes: Clarke transform, sliding mode observer, low-pass filter, position angle and speed estimation.

V. BASED ON SUPER-TWISTING CONTROLLER DESIGN

Super-twisting sliding mode control is derived from the second-order sliding mode control theory of high-order sliding mode. Its motion trajectory is a super-spiral curve and can reach convergence in a certain time. Super-twisting can not only maintain the fastness and robustness of first-order sliding mode control, but also effectively reduce the chattering generated by the sliding mode observer in vector control and enhance the stability of the system [20]–[22].

A. CONTROL PRINCIPLE OF SUPER-TWISTING ALGORITHM

Compared with the traditional second-order sliding mode control, Super-twisting sliding mode control structure is simple, the required variable information is small, and it is only related to the sliding mode variable s, no need to add new control quantity. It is a second-order sliding mode control algorithm that can be directly applied. In general, the nonlinear controlled system is [23], [24]:

$$\begin{cases} \dot{x} = a(x,t) + b(x,t)u \\ y = c(x,t) \end{cases} \tag{34}$$

In the above equation, x is the state variable of the system, u is the control input of the system, y is the output of the system, a and b are unknown and continuous sliding mode variable functions, and c is the unknown sliding surface function. The key point of the second order synovial control is to find a feedback control variable function u_1, so that the derivatives of the sliding mode surface function $c(x,t)$ and $c(x,t)$ can reach the origin of the phase plane in a finite time under the action of the control variable. That is, $y = \dot{y} = 0$, at this time, any bounded input in the system will converge to the sliding surface in a certain period of time.

From the equation (17), the second derivative of x can be obtained as:

$$\ddot{x} = A(x,t) + B(x,t)u_1 \tag{35}$$

where $A(x,t) = \ddot{x}|_{u_1=0}$; $B(x,t) = \frac{d\ddot{x}}{du_1} \neq 0$; A, B are continuous unknown functions, and there are positive integers A_{M}, B_{M}, B_{m} so that any x, u_1 are satisfied:

$$\begin{cases} |A| \leq \mathrm{A_M} \\ B_m \leq B \leq B_M \end{cases} \tag{36}$$

Set in any range, formula (19) satisfies:

$$\ddot{x} = [-A, A] + [Bm, B_M]\dot{u}_1 \tag{37}$$

Generally, the second-order sliding mode controller satisfies the form of equation (20) and satisfies $\dot{x} = 0, \ddot{x} = 0$ for a limited time. At the same time, because the controller does not contain other variables that change with time, it is

not sensitive to external disturbances and has strong robustness. At this point, the function of the sliding surface is first selected as: $s = x^* - x$. The feedback control function of Super-twisting sliding mode control can be converted into the following general form by equation (20):

$$\begin{cases} u_1 = -k_p|s|^r \tanh(s) + u_2 \\ \dot{u}_2 = -k_i \tanh(s) \\ \tanh(ax) = \dfrac{e^{ax} - e^{-ax}}{e^{ax} + e^{-ax}} \end{cases} \tag{38}$$

Since the hyperbolic tangent function is a continuous and smooth function, the hyperbolic tangent function tanh(x) can be used to reduce the chattering in the second-order sliding mode control by using the hyperbolic tangent function tanh(x) instead of the sign function sgn(x), where k_p, k_i is the positive gain to be set. In the design of the second-order sliding mode controller, it is often only necessary to know the information of the sliding modulus s, and it is not necessary to know the value of the first derivative of s. At the same time, the controller mainly has two components. The first term is a nonlinear discontinuous function of the sliding mode variable. The nonlinear variable can be changed by changing the index r. The second term is the integral value of the sliding mode variable, which makes the second order sliding mode control can effectively eliminate chattering compared with the first order sliding mode control, and does not receive the influence of parameter change and external interference, so that the system has strong robustness. At the same time, according to formula (36), the two conditions satisfy the following conditions:

$$\begin{cases} k_p > \dfrac{A_M}{B_m} \\ k_i \geq 2\dfrac{k_i B_m + A_M}{B_m} \end{cases} \tag{39}$$

Then the above formula is a necessary and sufficient condition for the Super-twisting sliding mode control system to converge and stabilize in a certain period of time.

B. CONTROLLER DESIGN BASED ON SUPER-TWISTING SLIDING MODE ALGORITHM

In this paper, a second-order sliding mode speed controller and current controller based on Super-twisting algorithm are designed. From the electromagnetic thrust equations of equations (5) and (6), we can get:

$$\frac{d^2\omega}{dt^2} = -\frac{B}{M}\frac{d\omega}{dt} - \frac{1}{M}\frac{dF_l}{dt} + \frac{3p\psi_f\pi^2}{2M\tau^2}\frac{di_q}{dt} \tag{40}$$

Combined with formula (18), it can be known: $A(x,t) = -\frac{B}{M}\frac{d\omega}{dt} - \frac{1}{M}\frac{dF_l}{dt}$, $B(x,t) = \frac{3p\psi_f\pi^2}{2M\tau^2}$, where B, M, τ, F_l, ψ_f are bounded quantities, and there are sufficient and necessary conditions for finite time convergence according to equation (19): $|A| \leq A_M$, $B_m \leq B \leq B_M$.

At this point, the function of selecting the speed sliding surface firstly:

$$s_\omega = \omega^* - \omega \tag{41}$$

Therefore, the second-order sliding mode speed controller based on the Super-twisting algorithm can be designed as:

$$\begin{cases} i_q = -k_p|s_\omega|^r \tanh(s_\omega) + i_{q1} \\ \dot{i}_{q1} = -k_i \tanh(s_\omega) \end{cases} \tag{42}$$

According to equation (22), the parameters k_p, k_i in the speed controller can be designed. Through the designed speed controller, during the operation of the motor with complicated external disturbances, the speed of the mover is closely followed by the given reference speed. Similarly, according to the current differential equation in equation (2), we can get:

$$\frac{d^2 i_q}{dt^2} = -\frac{R_s}{L_q}\frac{di_q}{dt} + \frac{L_d}{L_q}\frac{v\pi}{\tau}\frac{di_d}{dt} - \frac{\psi_f}{L_q}\frac{d\omega}{dt} + \frac{1}{L_q}\frac{du_q}{dt} \tag{43}$$

In the above formula, Rs, L_q, L_d, and ψ_f are bounded quantities, and the necessary and sufficient conditions for finite time convergence according to equation (36) exist: $|A| \leq A_M$, $B_m \leq B \leq B_M$.

At this point, the function of the current sliding surface is first selected as:

$$s_i = i_q^* - i_q \tag{44}$$

Therefore, the second-order sliding mode speed controller based on the Super-twisting algorithm can be designed as:

$$\begin{cases} u_q = -k_p|s_i|^r \tanh(s_i) + u_{q1} \\ \dot{u}_{q1} = -k_i \tanh(s_i) \end{cases} \tag{45}$$

According to equation (39), the parameters k_p, k_i in the speed controller can be designed.

The block diagram of the Super-twisting sliding mode controller designed according to equations (42) and (45) is shown in Figure 7:

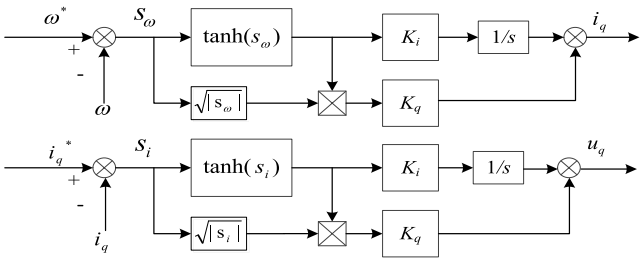

FIGURE 7. Super-twisting sliding mode controller.

VI. CONTROLLER DESIGN BASED ON SUPER-TWISTING

Compared with the traditional second-order sliding mode control, the Super-twisting sliding mode control structure is simple, the required variable information is small, and it is only related to the sliding mode variable s. It does not need to add a new control quantity, and it can be directly applied. However, in actual engineering, system boundary conditions are often fluctuated by external interference. When the system is in the sliding state, the uncertainty and disturbance of the matching are invariant. In order to obtain a good

control effect, the switching term gain needs to be adjusted when the system boundary changes, so the adaptive sliding mode algorithm has stronger anti-interference performance. Generally, in actual industrial control, the boundary of the system is difficult to determine, so the adaptive super-twisting algorithm has strong engineering significance.

According to equation (18), the controlled system that is disturbed is:

$$\ddot{x} = A(x,t) + B(x,t)u_1 + \varphi(t) \tag{46}$$

where, $\varphi(t)$ is a continuous random disturbance with no defined boundary, and u_1 is the control law of the Super-twisting algorithm. The Super-twisting speed feedback control function designed according to formula (42) is:

$$\begin{cases} i_q = -k_p |s_\omega|^r \tanh(s_\omega) + i_{q1} \\ \dot{i}_q 1 = -k_i \tanh(s_\omega) \end{cases}$$

where $k_p > 0, k_i > 0$, which are parameters that need to be designed in the Super-twisting control algorithm. Suppose the interference $\phi(t)$ is differentiable, and $\left|\dot{\phi}(t)\right| \leq \delta$, $\forall t \geq 0$, where δ is a normal number. Design a suitable adaptive control strategy to derive k_p and k_i such that $\dot{x}$ and $\ddot{x}$ converge to zero in a finite time. The adaptive laws for designing k_p and k_i are:

$$\dot{k}_p = \begin{cases} w_1 \sqrt{\frac{\gamma_1}{2}}, & x \neq 0 \\ 0, & x = 0 \end{cases} \tag{47}$$

$$k_i = \chi + \frac{\eta^2}{4} + \frac{k_p \eta}{4} \tag{48}$$

where, $\eta > 4$, χ, γ_1 and w_1 are all positive numbers. By constructing the quadratic Lyapunov function [17], the boundedness of the designed adaptive parameters can be proved. When $\dot{x} = \ddot{x} = 0$ in the control system, the parameters k_p and k_i remain fixed. When the system does not reach the sliding surface, during the control adjustment, the parameters k_p and k_i do the constant-speed variable movement, thus continuously improving the control effect. A more detailed derivation process in [25] proves that under the above parameters, x1 and x2 can converge to zero in a finite time. The structure diagram of the adaptive Super-twisting sliding mode speed controller designed according to the above formula is shown in Figure 8.

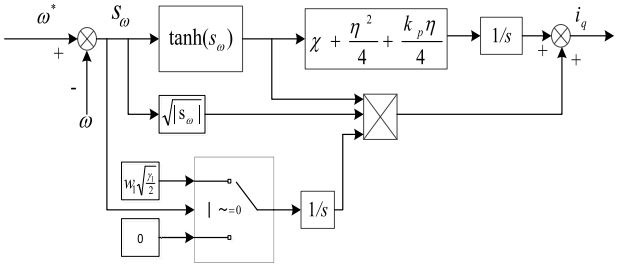

FIGURE 8. Adaptive Super-twisting sliding mode speed controller.

The block diagram of the control system is shown in Figure 9. By measuring the three-phase current values i_a, i_b, i_c and the three-phase voltage values u_a, u_b, u_c in

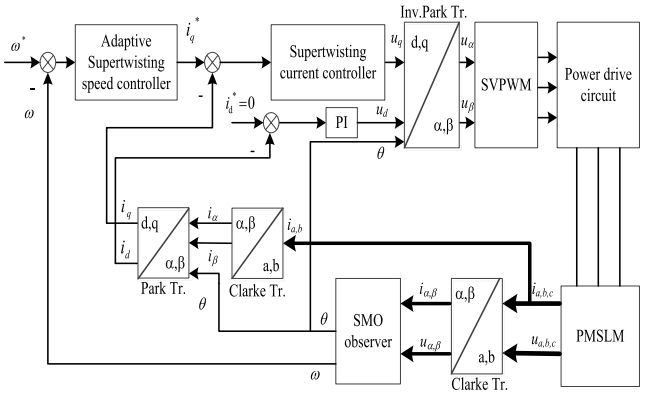

FIGURE 9. Control system structure.

the inverter as input to the sliding mode observer SMO. Observing the back electromotive forces e_α, e_β in the motor operation through the state observer, the required estimated ω_r and θ can be obtained through a series of calculations. According to the error between the observe ω_r^* and the given ω_r, i_q^* is obtained by Self-adaptive Super-twisting sliding mode speed controller. Then, the observed $\theta*$ and three-phase currents are introduced into the vector transformation, and the obtained feedback value of i_q is made to be different from the given value i_q*, and u_q is obtained by the super-twisting sliding mode current controller. The target voltage vector is synthesized by the inverse Park transform and the SVPWM module, and then the driving circuit controls the operation of the PMSLM.

TABLE 1. Main parameters of permanent magnet synchronous linear motor.

Parameter meaning	Value
Stator resistance Rs	4.0Ω
D-axis inductance Ld	8.2 mH
Q-axis inductance Lq	8.2 mH
Moment mass m	1.425kg
Viscous friction coefficient B	44N·m·s
Pole distanceτ	0.016m
DC bus voltage V	48v
Continuous thrust F	32N

VII. SIMULATION ANALYSIS

The block diagram of the control system of the permanent magnet synchronous linear motor without sensor vector control based on Self-adaptive Super-twisting sliding mode controller is shown in Figure 9. According to the simulation model built by the motor drive parameters shown in Table 1, the ability of different observers to track the speed and position of the linear motor is analyzed, so that the best observer can be selected to obtain the position and speed of the linear motor mover. And combined with the selected observer to design different controllers, adjust the controller structure and parameters to obtain the best control performance.

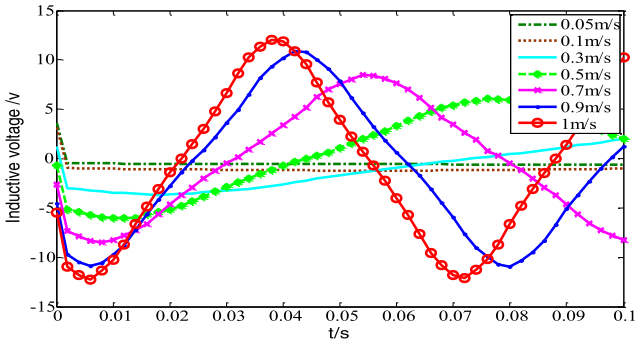

FIGURE 10. Induced voltage at different speeds.

A. ANALYSIS OF BACK ELECTROMOTIVE FORCE OF LINEAR MOTOR

When the linear motor is subjected to sensorless control research, its mover position information is hidden in the back EMF of the motor. This paper mainly constructs the sliding mode state observer to obtain the linear back EMF, and then analyzes the motor mover position information. In the finite element simulation analysis, a curve diagram of the back EMF due to the difference in motor speed can be obtained. By analyzing Figure 10, when the motor running speed is higher than 0.5m/s, the back EMF of the motor exhibits an approximately sinusoidal change. When the speed is low, the back EMF amplitude is low and the waveform is chaotic. In engineering applications, it is likely to be annihilated in the electrical interference signal, which is difficult to actually observe. Therefore, for a sensorless control strategy based on extracting a mover position signal from the back EMF information, it is suitable for medium and high speed motors, and this strategy is not applicable for motors that need to operate in a lower speed environment. The research object of this paper is a linear motor with fast response and high precision. It is mainly used in medium and high speed working environment such as rail transit and machine tool processing. Therefore, the sensorless control strategy based on sliding mode control algorithm can meet the requirements of linear motor. Most occasions require.

B. POSITION SPEED TRACKING UNDER DIFFERENT OBSERVER

In order to determine the ability of different observers to track the position and speed of the permanent magnet synchronous linear motor during operation, the traditional sliding mode state observer (SMO), extended Kalman state observer (Kalman) and improved sliding mode are designed respectively. The state observer (E-SMO) is simulated under the regulation of the speed and current double closed-loop PI controller.

Linear motors often perform uniform switching motions and uniform acceleration switching motions in industrial applications. Repeated switching movements will cause the speed direction to suddenly change, and the motor current will be distorted. The observer's tracking of speed and

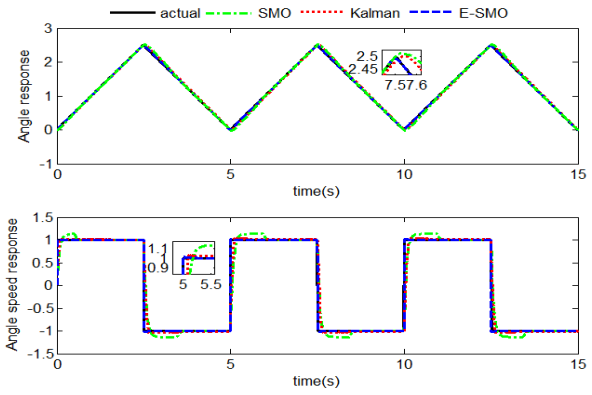

FIGURE 11. Uniform speed switching speed and position tracking.

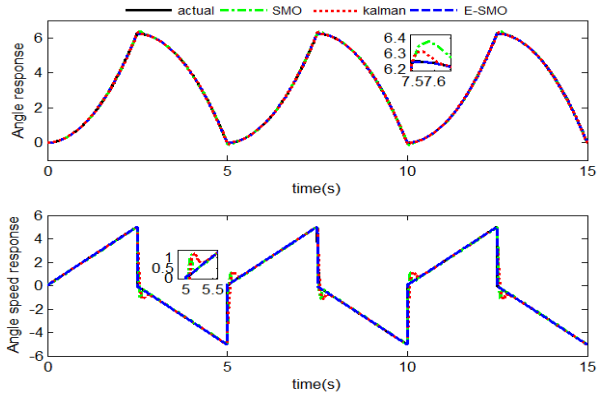

FIGURE 12. Uniform acceleration switching motion speed and position tracking.

position depends on the calculation of current and back EMF, which will have a significant impact on the state observer. In the simulation experiment, the switching motion of the actual motor is simulated. The tracking ability of each observer for position and speed is shown in Figure 11 and Figure 12. In the constant speed switching movement, the speed is set to 1m/s, and the speed is reversed after 5s. At the switching point, it can be found that the traditional sliding mode observer does not perform angle compensation, and generates large jitter when the speed is reversed and the current is distorted, and the tracking effect at the switching point is not good. In the uniform acceleration switching motion, the degree of distortion of the current at the switching point is more serious than that at the constant speed switching. Due to the serious dependence of the extended Kalman observer on the ontology mathematical model, the amount of calculation is large, and the distortion signal cannot be corrected in time to produce a large deviation. The improved sliding mode state observer adds low-pass filtering and is immune to current distortion signals. By using the hyperbolic tangent function tanh(x) instead of the symbol function sgn(x) as the switching function, the chattering in the tracking process can be effectively reduced, and the tracking ability of the linear motor is better.

C. RESEARCH ON SENSORLESS CONTROL STRATEGY UNDER DIFFERENT CONTROLLERS

Since the improved sliding mode state observer has better tracking ability for the position and velocity of the straight line, the improved sliding mode state observer is selected to replace the traditional sensor to generate the position and velocity feedback signals. At the same time, the speed loop and current loop based on PI controller are designed to form a double closed loop control system, and compared with the double closed loop speed control system based on adaptive Super-twisting speed controller and Super-twisting current controller. Compare the system's ability to resist load changes and suppress structural perturbations caused by sliding mode observers. The comparison results are shown in Figure 13.

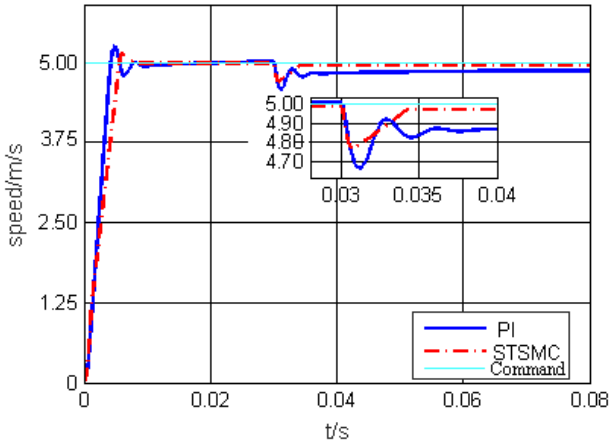

FIGURE 13. Speed tracking under PI and STSMC control.

It can be seen from Figure 13 that the given speed is 5 m/s and the load is suddenly increased at 0.03 s. Based on the Super-twisting controller (STSMC), the motor has less chattering and robustness during the running to a given speed. At the same time, its load-resistance is significantly enhanced compared with the PI controller, and finally reaches the given speed has excellent control effect, indicating that the second-order sliding mode structure of Super-twisting controller does have stronger convergence and anti-interference ability.

However, during the operation of the linear motor, the influence of its end effect and the influence of the electrical parameters during the traveling process on the system will interfere with the system operation. And many disturbances have the characteristics of uncertainty boundaries, so the controller needs to be improved to solve the above problems. In this paper, an adaptive Super-twisting sliding mode speed controller (Self-adaptive STSMC) is designed. The adaptive structure can automatically adjust the controller parameters according to the variable boundary disturbance, which can play a dynamic adjustment role and can effectively improve the system robustness.

After adding the uncertainty boundary disturbance inside the system, the speed control performance comparison between the STSMC control structure and the Self-adaptive STSMC control structure is shown in Figure 14. The convergence diagrams of the speed sliding surface and the current sliding surface are shown in Figure 15 and Figure 16, respectively. The adaptive system dynamically adjusts its control parameters according to the disturbances it receives, as shown in Figure 17.

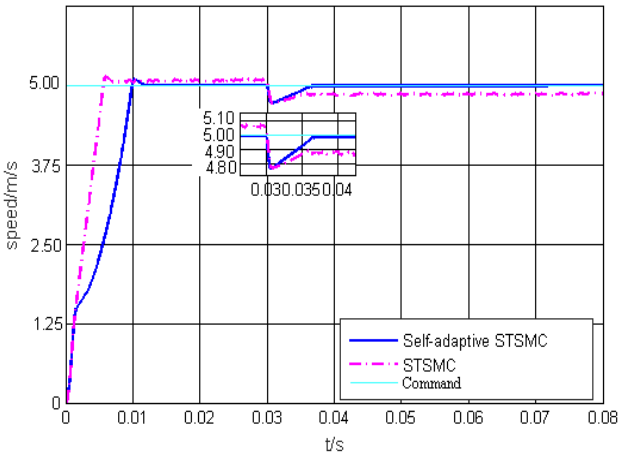

FIGURE 14. Speed tracking under the control of self-adaptive STSMC and STSMC.

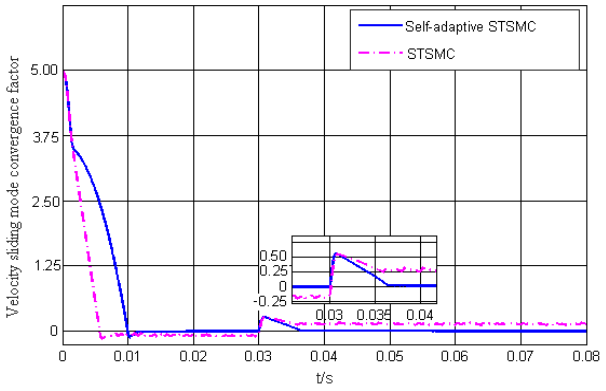

FIGURE 15. Speed sliding surface controlled by self-adaptive STSMC and STSMC.

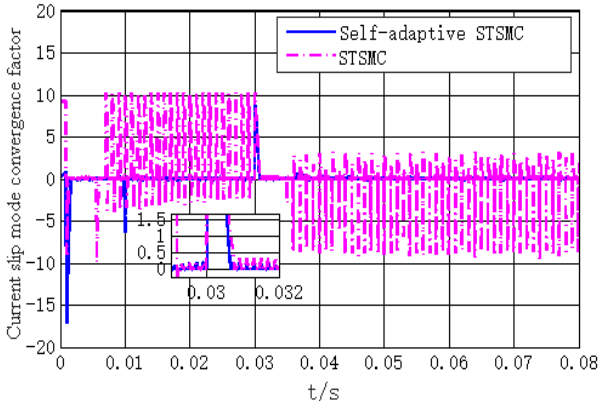

FIGURE 16. Current sliding surface controlled by self-adaptive STSMC and STSMC.

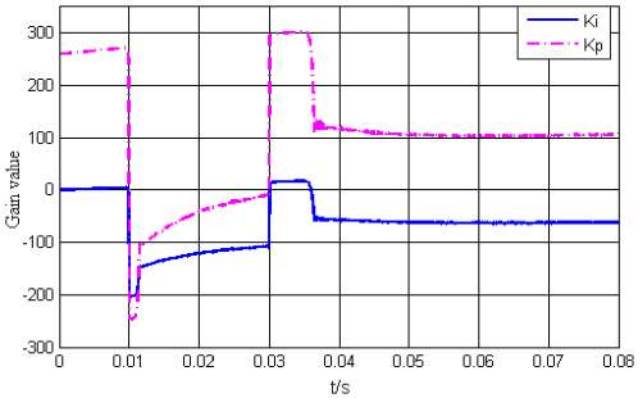

FIGURE 17. Parameters k_i and k_p of self-adaptive STSMC.

In the actual industrial production process, the operating environment is complex, the external disturbance is frequent, and the internal electrical parameters are unstable. In order to better close to the actual operating environment of the motor, this paper adds a boundary-free continuous random disturbance to the simulation platform. From the above simulation results (Figure 14-16), it can be found that after the addition of the boundaryless random disturbance, under the action of the STSMC controller, the motor is running under the disturbance due to the poor robustness and adaptability of the system. The sliding surface of the speed and current during the process produces a large chattering. Under the control of the adaptive Super-twisting controller (Self-adaptive STSMC), the system has strong anti-disturbance capability. Under continuous boundaryless random disturbance, the speed fluctuation is small and the system runs smoothly (Figure 14). From the speed sliding surface of the two, as shown in Figure 15, the Self-adaptive STSMC system can completely converge to zero at a faster speed under disturbance. In the overall motor control system, the current loop acts as the inner loop. The changes of various electrical parameters directly affect the current change, and its structural characteristics make it susceptible to disturbance. As shown in Figure 16, under the continuous random disturbance without boundary, STSMC The current sliding surface of the control system is violently shaken, and the stability of the system is poor. The current sliding surface of the Self-adaptive STSMC system changes smoothly and converges to zero quickly. The chattering vibration is small during the whole operation of the system, and the speed tracking ability is strong, which can suppress the external disturbance better, which proves that the structure has good robustness and strong adaptability.

Under the action of continuous random external disturbance and load disturbance without boundary, the adaptive laws of k_p and k_i are designed according to formula (47) and formula (48). As shown in Figure 17, the adjustment curves of the parameters k_p and k_i are suppressed. The Self-adaptive STSMC controller automatically adjusts controller parameters based on the disturbances it receives, speeds up system stabilization and increases system immunity.

FIGURE 18. Permanent magnet synchronous linear motor.

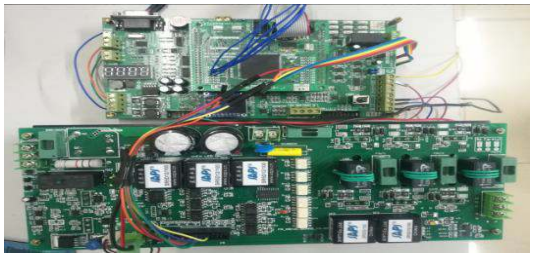

FIGURE 19. Control and drive circuit.

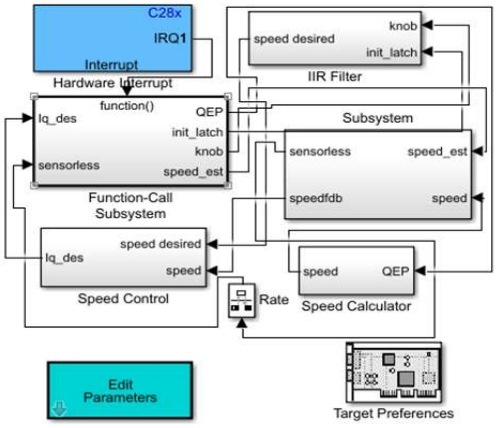

FIGURE 20. Code model diagram.

VIII. EXPERIMENTAL VERIFICATION

In order to verify the effectiveness of the sensorless vector control method for permanent magnet synchronous linear motor based on adaptive Super-twisting sliding mode controller, the experimental platform of permanent magnet synchronous linear motor system is constructed, as shown in Fig. 18 and Figure 19. The system uses TI's TMS320F28335 digital processing chip to achieve control. The controlled motor speed sensor is retained for speed comparison and verification. The motor parameters in the experiment are consistent with the simulation. The model-based design method is used to design the embedded code. Figure 20 shows a schematic diagram of the code model. At the same time, the MBD design toolbox supported by TI is used to design the upper layer software, and then the code is optimized and then analyzed.

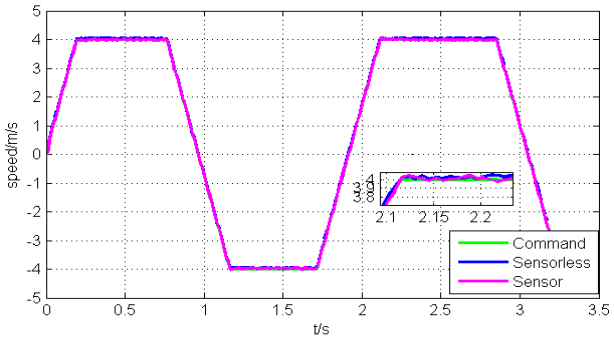

FIGURE 21. Comparison between non-sensing strategy and switching speed tracking under speed sensor.

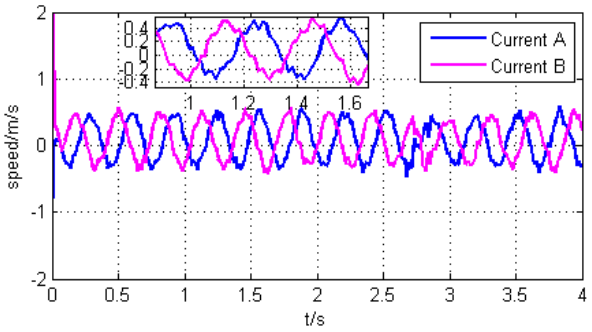

FIGURE 22. Switching motion current waveform under PI control.

The measurement error and electrical interference in the experiment are very different from the ideal simulation environment. It is difficult to extract and observe the back EMF of the linear motor at lower speed, which makes it difficult to obtain the motor running speed and position. In order to achieve reliable operation of the motor, the linear motor was set at a speed of 4 m/s and was tested under light load conditions. The speed of the motor is tracked at a given speed of 4 m/s, and the speed of the motor is compared with the speed of the actual speed sensor based on the sensorless vector control strategy of the adaptive super-twisting sliding mode controller based on the disturbance observer. As shown in Figure 21. It can be seen from Figure 21 that under the specified speed command, the permanent magnet synchronous linear motor adopts the adaptive super-twisting sliding mode controller's sensorless vector control strategy, which makes the system have good speed regulation capability and speed buffeting. Smaller, compared with the application of the actual speed sensor as the position feedback control method, has the same excellent speed control effect.

Figure 22 shows the current waveform when the linear motor is subjected to switching motion under PI control when it is disturbed by the outside world. It can be seen from the figure that under the influence of the application of continuous uncertainty boundary disturbance, the A and B phase current waveforms will produce significant chattering, and the A and B phase drive currents will be significantly distorted at the speed switching point. However, it is stable

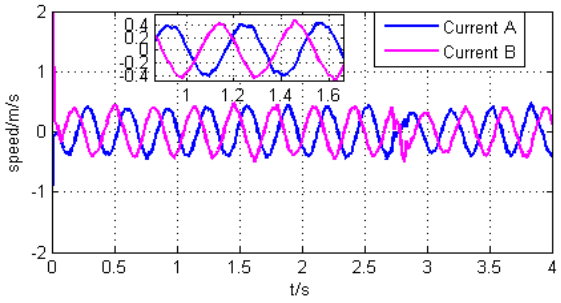

FIGURE 23. Switching motion current waveform based on Self-adaptive super-twisting sliding mode control.

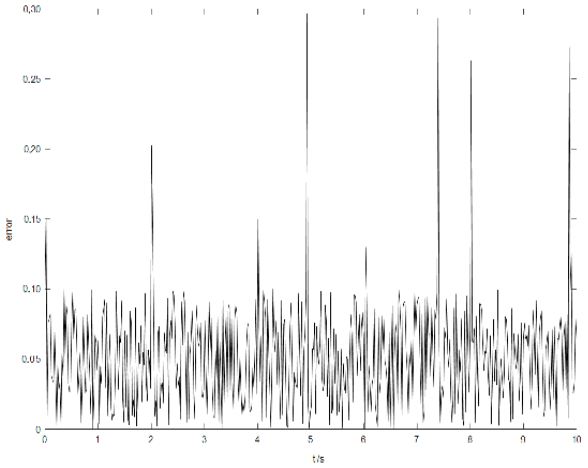

FIGURE 24. Speed error between rotational speed and given speed under PI control.

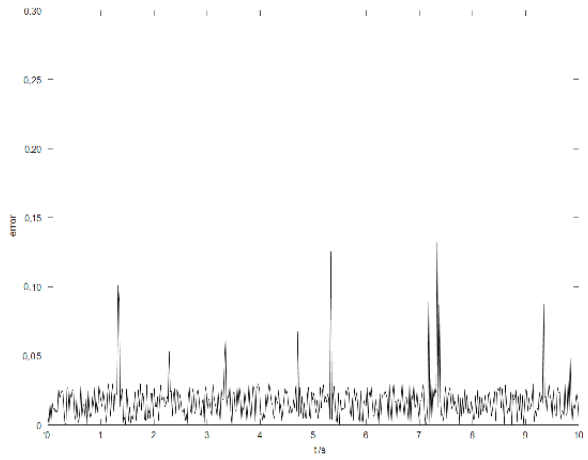

FIGURE 25. Speed error between the speed and the given speed under Self-adaptive STSMC control.

and stable under the action of the controller, indicating that this control strategy has a fast response speed and has a certain inhibitory effect on the disturbance. Figure 23 shows the linear motor maintained in the same operating environment as Figure 22. The speed controller at this time uses the Self-adaptive STSMC controller. The A and B phase current waveforms are still very smooth during the

continuous interference. The current distortion at the switch is obvious, but it can recover smoothly and quickly under the action of the controller. This shows that under the control of the Self-adaptive STSMC controller, it is more robust and adaptable than other control systems.

It can be seen from Figure 24 that when the linear motor is disturbed by the outside, the speed error between the speed under the PI control and the given speed fluctuates greatly, which proves that the control strategy has insufficient ability to suppress the disturbance. Figure 24 maintains the same operating environment as Figure 25. At this time, the speed controller of the linear motor adopts the Self-adaptive STSMC controller. It can be seen that this control strategy can effectively suppress external disturbances, and the speed error fluctuation is small, indicating The robustness and adaptability of the system are enhanced by the Self-adaptive STSMC controller, which effectively improves the overall control performance of the linear motor.

IX. CONCLUSION

In this paper, based on the research of sensorless control strategy of Self-adaptive Super-twisting sliding mode linear motor, according to the analysis of the back electromotive force waveform of linear motor in finite element software, the improved sliding mode state observer is replaced by the high speed operation of the motor. The speed sensor adopts a hyperbolic sinusoidal switching function in the improved sliding mode observer, which effectively reduces the chattering of the system. At the same time, the Self-adaptive Super-twisting sliding mode control scheme can effectively suppress the influence of the uncertain boundary disturbance in the system and reduce the chattering. This solution improves the overall robustness and adaptability of the system. And it is fully verified on the simulation and experimental platform that the control strategy can effectively realize the sensorless control scheme for the permanent magnet synchronous linear motor, which not only optimizes the structure of the linear motor, but also improves the control performance of the motor in non-sensing state.

REFERENCES

[1] M. Yahiaoui, A. Kechich, and I. K. Bouserhane, "Adaptive sliding mode control of PMLSM drive," *Int. J. Power Electron. Drive Syst.*, vol. 8, no. 2, pp. 639–646, 2017.
[2] G. S. Vompolu, K. Abhishek, and N. C. Lenin, "Design and development of permanent magnet linear synchronous motor (PMLSM)," *Indian J. Sci. Technol.*, vol. 10, no. 27, pp. 1–4, 2017.
[3] X. Liu, J. Gao, S. Huang, and K. Lu, "Magnetic field and thrust analysis of the U-channel air-core permanent magnet linear synchronous motor," *IEEE Trans. Magn.*, vol. 53, no. 6, Jun. 2017, Art. no. 8201504.
[4] Z. Qiao, T. Shi, Y. Wang, Y. Yan, C. Xia, and X. He, "New sliding-mode observer for position sensorless control of permanent-magnet synchronous motor," *IEEE Trans. Ind. Electron.*, vol. 60, no. 2, pp. 710–719, Feb. 2013.
[5] X. Zhang, B. Hou, and Y. Mei, "Deadbeat predictive current control of permanent-magnet synchronous motors with stator current and disturbance observer," *IEEE Trans. Power Electron.*, vol. 32, no. 5, pp. 3818–3834, May 2017.
[6] G. Wanli, H. Yunfeng, and Z. Sen, "Design and experiment of adaptive sliding mode controller for brushed DC motor," (in Chinese), *J. Xi'an Jiaotong Univ.*, vol. 9, no. 7, pp. 123–125, 2017.
[7] Y. Feng, X. Yu, and F. Han, "High-order terminal sliding-mode observer for parameter estimation of a permanent-magnet synchronous motor," *IEEE Trans. Ind. Electron.*, vol. 60, no. 10, pp. 4272–4280, Oct. 2013.
[8] A. Levant, "Principles of 2-sliding mode design," *Automatica*, vol. 43, no. 4, pp. 576–586, 2007.
[9] Y. Xin, C. Changchun, Z. Jinzhong, and L. Mingming, "Sensorless direct torque control of permanent magnet synchronous motor using a super-twisting controller," (in Chinese), *J. Shanghai Dianji Univ.*, vol. 20, no. 3, pp. 140–146, 2017.
[10] M. A. G. Moghadam and F. Tahami, "Sensorless control of PMSMs with tolerance for delays and stator resistance uncertainties," *IEEE Trans. Power Electron.*, vol. 28, no. 3, pp. 1391–1399, Mar. 2013.
[11] Y. Zhang, Z. Yang, M. Yu, K. Lu, Y. Ye, and X. Liu, "Analysis and design of double-sided air core linear servo motor with trapezoidal permanent magnets," *IEEE Trans. Magn.*, vol. 47, no. 10, pp. 3236–3239, Oct. 2011.
[12] H. Zhou, Z. Lu, W. Zhao, G. Liu, and L. Xu, "Design and analysis of low-cost tubular fault-tolerant interior permanent-magnet motor," *IEEE Trans. Magn.*, vol. 52, no. 7, Jul. 2016, Art. no. 8104804.
[13] S. J. Kim, E. J. Park, S. Y. Jung, and Y. J. Kim, "Optimal design of reformed auxiliary teeth for reducing end detent force of stationary discontinuous armature PMLSM," *IEEE Trans. Appl. Supercond.*, vol. 26, no. 4, pp. 1–5, Jun. 2016.
[14] Z.-J. Zhang, M.-Z. Luo, B.-Q. Kou, and C.-Q. Luo, "Characteristic analysis of a trilateral permanent magnet linear synchronous motor with slotless ring windings," *IET Elect. Syst. Transp.*, vol. 8, no. 1, pp. 20–26, 2018.
[15] H. Du, X. Chen, G. Wen, X. Yu, and J. Lü, "Discrete-time fast terminal sliding mode control for permanent magnet linear motor," *IEEE Trans. Ind. Electron.*, vol. 65, no. 12, pp. 9916–9927, Dec. 2018.
[16] S.-A. Kim, Y.-W. Zhu, S.-G. Lee, S. Saha, and Y.-H. Cho, "Electromagnetic normal force characteristics of a permanent magnet linear synchronous motor with double primary side," *IEEE Trans. Magn.*, vol. 50, no. 1, Jan. 2014, Art. no. 4001204.
[17] P. Yuedou, C. Tao, and C. Zeping, "Design of stator flux observer for induction motor super-twisting algorithm," (in Chinese), *J. Electr. Mach. Control*, vol. 20, no. 5, pp. 61–67, 2016.
[18] H. Kim, J. Son, and J. Lee, "A high-speed sliding-mode observer for the sensorless speed control of a PMSM," *IEEE Trans. Ind. Electron.*, vol. 58, no. 9, pp. 4069–4077, Sep. 2011.
[19] M. Ezzat, A. Glumineau, and F. Plestan, "Sensorless high order sliding mode control of permanent magnet synchronous motor," in *Proc. 11th Int. Workshop Variable Struct. Syst.*, Jun. 2010, pp. 233–238.
[20] L. Yuan, F. Xiao, J.-Q. Shen, M.-L. Chen, Q.-M. Shi, and L. Quan-Feng, "Sensorless control of high-power interior permanent-magnet synchronous motor drives at very low speed," *IET Electr. Power Appl.*, vol. 7, no. 3, pp. 199–206, Mar. 2013.
[21] D. Liang, J. Li, and R. Qu, "Sensorless control of permanent magnet synchronous machine based on second-order sliding-mode observer with online resistance estimation," *IEEE Trans. Ind. Appl.*, vol. 53, no. 4, pp. 3672–3682, Jul./Aug. 2017.
[22] G. Ruyuan and D. Fujun, "Design of permanent magnet synchronous motor torque ring controller based on super-twisting sliding mode," (in Chinese), *Micromotor*, vol. 51, no. 2, pp. 52–68, 2018.
[23] W. Dongling, Z. Chaohui, W. Feiyu, and S. Qiang, "Speed and torque control based on super-twisting sliding mode permanent magnet synchronous motor," (in Chinese), *Motor Control Appl.*, vol. 44, no. 10, pp. 42–47, 2017.
[24] M. Ezzat, A. Glumineau, and F. Plestan, "Sensorless speed control of a permanent magnet synchronous motor: High order sliding mode controller and sliding mode observer," *Proc. IFAC*, vol. 43, no. 14, pp. 1290–1295, 2010.
[25] Y.-B. Sun, X. Yang, J.-K. Xia, and C.-Y. Wang, "Second order sliding mode control of PMLSM based on diagonalization method," (in Chinese), *Proc. Chin. Soc. Elect. Eng.*, vol. 28, no. 12, pp. 124–128, 2008.

ZHENG LI was born in Shijiazhuang, China, in 1980. He received the Ph.D. degree in power electronics and electrical drive from the Hefei University of Technology, China, in 2007.

He is currently a Professor with the Hebei University of Science and Technology, Shijiazhuang. He has authored more than 160 published papers. His major research interests include design, analysis, and control of novel motors and actuators, intelligent control, smart grid, and power electronics.

SHUO ZHOU was born in Zhuozhou, China, in 1994. She received the bachelor's degree in electrical engineering and automation from Hebei Science and Technology Normal University, in 2018. She is currently pursuing the master's degree with the Hebei University of Science and Technology.

She is currently a graduate student with the Hebei University of Science and Technology. Her research interests include linear motor control algorithm and motor drive.

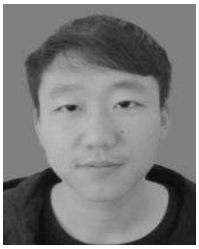

YU XIAO was born in Chengde, China, in 1995. He received the bachelor's degree in automation from the Hebei University of Science and Technology, in 2018, where he is currently pursuing the master's degree.

He is currently a graduate student with the Hebei University of Science and Technology. His research interests include special motor control and linear motor drive.

LEIYONG WANG was born in Shijiazhuang, China, in 1984. He received the degree in automation from the Shenyang Institute of Engineering, in 2007. He is currently pursuing the master's degree with the Hebei University of Science and Technology.

He is currently a graduate student with the Hebei University of Science and Technology. His research interests include special motor control and linear motor drive.